J Appl Electrochem (2011) 41:1245–1252
DOI 10.1007/s10800-011-0347-3

ORIGINAL PAPER

Analysis of a gas-phase Br_2–H_2 redox flow battery

Rui Zhang · John W. Weidner

Received: 12 May 2011 / Accepted: 16 August 2011 / Published online: 31 August 2011

Abstract The operation of a gas-phase Br_2–H_2 flow battery is analyzed via a mathematical model and compared to experimental data. The model predicts the operating conditions of the cell in both fuel-cell (i.e., discharge) and electrolysis (i.e., charge) mode as a function of current, inlet gas composition, flow rate, and pressure differential across the membrane. The analysis reveals that gas-phase Br_2/HBr reactants significantly enhance mass transfer, which enables higher currents densities to be achieved compared to a liquid-fed system. A key feature of the model is water transport across the membrane, which determines membrane conductivity, reactant concentration and undesired condensation. The model is used to provide insight into cell operation, including operating conditions needed to avoid water condensation.

Keywords Br_2–H_2 flow battery · Mathematical model · Mass transfer · Efficiency

List of symbols

A	Area of membrane, cm^2
C_i^s	Surface concentration of species *i*, mol/cm^3
C_i^{eq}	Equilibrium concentration of species *i*, mol/cm^3
D_i	Diffusion coefficient of species *i*, cm^2/s
d	Depth of the flow channel, cm
F	Faraday's constant, 96,485 C/equiv
i	Current density, A/cm^2
i_{app}	Applied average current density, A/cm^2
i_0	Exchange current density, A/cm^2
L_c	Location of condensing point, cm
L	Total length of the electrode channel, cm
M_M	Molecular weight of Nafion membrane, g/mol
N_i	Molar flux of species *i*, $mol/(cm^2\ s)$
P_M	Membrane permeability, mol/(cm s kPa)
P	Electrode pressure, kPa
r	Molar ratio of Br_2 to HBr, $\left(y_{Br_2}/y_{HBr}\right)$
R	Ideal gas constant, 8.314 J/(K·mol)
R_A	Membrane area resistance, Ω—cm^2
T	Temperature, K
U_{eq}	Equilibrium cell potential, V
U_{eq}^0	Equilibrium cell potential at standard conditions, V
V_{cell}	Cell voltage, V
V_L	Superficial velocity of condensate, cm/s
w	Width of the flow channel, cm
$x_{w,e}$	Mole fraction of water in liquid phase at dew point
$y_{w,e}$	Mole fraction of water in vapor phase at dew point
y_i	Mole fraction of species *i* in the vapor phase

Greek

α	Transfer number for the HBr oxidation
β	Transfer number for the Br_2 reduction
δ_0	Thickness of condensate at exit, cm
δ_z	Thickness of condensate at location z, cm
η	Activation overpotential of the electrodes, V
ρ	Density of the condensate, g/cm^3
δ_M	Thickness of Nafion membrane, cm
λ	Water content of the Nafion membrane
ξ	Electro-osmotic drag coefficient, H^+/H_2O
μ	Viscosity of the condensate, g/(cm·s)

Subscripts

+	Positive electrode, HBr/Br_2 side
−	Negative electrode, H^+/H_2 side
ch	Charge

R. Zhang · J. W. Weidner (✉)
Department of Chemical Engineering, Center for Electrochemical Engineering, University of South Carolina, Columbia, SC 29208, USA
e-mail: weidner@cec.sc.edu

dis Discharge
i Species
w Water
x Distance across the membrane, cm
z Distance in the flow direction channel, cm

1 Introduction

Redox flow batteries are attractive devices for large scale energy storage for capturing the inherent fluctuations in renewable energy [1–3]. These devices use the redox states of various chemical couples (e.g., iron-chromium, vanadium systems, zinc-bromine) to efficiently cycle between the charge and discharge states. As in a fuel cell, the energy conversion device is separated from the energy storage containers enabling energy and power to be optimized independently for a given application. One potentially interesting redox couple is the Br_2–H_2 system due to good reversibility of the reactions and fast recharge rates [4–7]. However, liquid-based bromine cells operate at low power. For example, limiting currents of 40–60 mA/cm^2 in 0.2–0.3 M Br_2 was found in the Zn–Br_2 flow cell [6, 7]. Although the sluggish solid zinc electrode is a problem in this system, theoretical studies by Mader and White [8] reveal that the limiting current on the bromine electrode is less than 100 mA/cm^2 due to low bromine solubility and liquid-phase diffusion.

To increase power, and hence decrease size and cost of the energy conversion device, we developed a gas-phase Br_2 positive electrode to replace the liquid-phase electrode [9]. The gas-phase system greatly minimizes mass-transfer resistance, as we observed in our HCl [10, 11] and HBr [12, 13] electrolyzer systems. In the Br_2–H_2 flow battery (see Fig. 1), the reactions at the positive and negative electrode are shown in Eqs. 1 and 2, respectively.

$$2\mathrm{HBr(g)} \underset{\text{Discharge}}{\overset{\text{Charge}}{\longleftrightarrow}} \mathrm{Br_2(g)} + 2\mathrm{H^+} + 2\mathrm{e^-} \quad (1)$$

$$2\mathrm{H^+} + 2\mathrm{e^-} \underset{\text{Discharge}}{\overset{\text{Charge}}{\longleftrightarrow}} \mathrm{H_2} \quad (2)$$

At the positive electrode, a mixture of gaseous HBr, Br_2 and H_2O are fed into the flow battery. Bromine is consumed on discharge (i.e., fuel-cell mode) and produced on charge (i.e., electrolyzer mode). At the negative electrode, a mixture of gaseous water and hydrogen are fed and hydrogen is consumed and produced on discharge and charge, respectively. The overall reaction is:

$$2\mathrm{HBr(g)} \underset{\text{Discharge}}{\overset{\text{Charge}}{\longleftrightarrow}} \mathrm{Br_2(g)} + \mathrm{H_2(g)} \quad (3)$$

Although water does not participate in the reaction, it is a critical component during cell operation if a membrane such as Nafion® is used. These membranes must remain hydrated in order to conduct protons. Water can be transported across the membrane via three mechanisms: (1) diffusion due to a water activity gradient; (2) electroosomtic drag due to the flow of protons (i.e., current); and (3) permeation due to a pressure differential. If the concentration of water vapor exceeds the dew point on either electrode, condensation can occur. For illustration, Fig. 1 shows the formation of an aqueous layer of HBr and Br_2 at the positive electrode. This layer forms at the saturation point in the cell (designated by $z = L_c$) and grows in thickness in the gas-diffusion layer until the liquid exits the cell at $z = L$. This liquid layer inhibits the transport of reactants to the catalyst/membrane interface.

In this paper, the operation of a gas-phase Br_2–H_2 flow battery is analyzed via a mathematical model and compared to experimental data. The model predicts the operating conditions of the cell in both charge and discharge mode as a function of current, inlet gas composition, flow

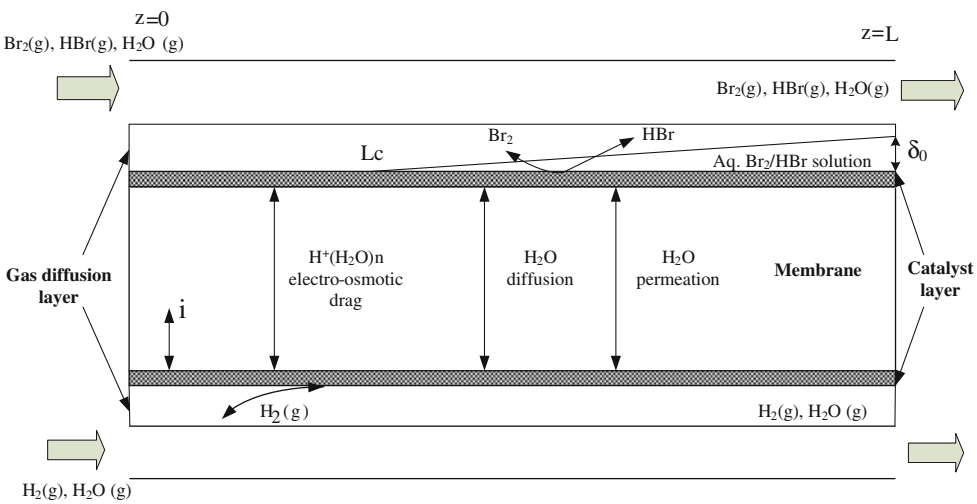

Fig. 1 Schematic of the reactions and transport occurring in the Br_2–H_2 redox flow battery. Direction of the electrode reactions depends on the current direction, according to Eqs. 1 and 2. The direction of water transport via the three transport mechanisms depends on the operating conditions of the cell. Also shown is a liquid aqueous HBr/Br_2 layer that forms at the saturation point in the cell ($z = L_c$) and grows in thickness in the gas-diffusion layer until the liquid exits the cell at $z = L$

rate, and pressure differential across the membrane. A key feature of the model is water transport, which determines membrane conductivity, reactant concentration and undesired condensation. The model is used to provide insight into cell operation, including operating conditions needed to avoid water condensation.

2 Model developments

The cell voltage is composed of the equilibrium cell potential, ohmic losses across the membrane, and overpotentials at each electrode, as shown below.

$$V_{cell} = U_{eq} + iR_A + \eta_+ - \eta_- \quad (4)$$

The anode and cathode overpotentials are defined as positive and negative, respectively, and the current density is positive on charge and negative on discharge. Also assumption in writing Eq. 4 is that crossover of reactants does not affect the cell voltage via a mixed potential. Acid crossover is expected to be very small in a proton-exchange membrane, and this was confirmed for HCl [10] and H_2SO_4 [14]. Bromine crossover is based on its solubility and diffusion through Nafion membrane, and these values will be on the order of those for water. Based on the solubility and diffusion coefficient for Br_2 in water found from OLI and used here, the crossover current is expected to be less than 1 mA/cm^2. At the small current perturbations applied previously to the H_2/Br_2 system (<60 mA/cm^2 [9]), crossover was not an issue. Therefore, even with a pressure differential of tens of atmospheres, crossover should not greatly affect cell voltage at the high currents desired for this system. For large-scale installations though, even low crossover rates could prove problematic for other reasons and this would warrant further study.

When all reactants and products are in the gas phase, the equilibrium cell potential is calculated from the Nernst Equation shown below [9].

$$U_{eq} = U^0_{eq} - \frac{RT}{2F}\ln\left[\frac{y_{H_2}y_{Br_2}}{y^2_{HBr}}\right] \quad (5)$$

Equation 5 assumes that the activity of reactants and products are ideal and given by the gas-phase mole fractions. This was confirmed by the OLI software for the H_2O–HBr–Br_2 system [15].

Since water is on both sides of the cell, the mole fractions of the gases in Eq. 5 must account for water such that the follow relationships hold on the positive and negative electrodes, respectively:

$$y_{w+} + y_{Br_2} + y_{HBr} = 1 \quad (6)$$

$$y_{w-} + y_{H_2} = 1 \quad (7)$$

To calculate the water composition on the positive electrode, a water balance along the length of the flow channel (i.e., z-direction) developed previously is used [10, 14].

$$\frac{dN_{w,z}}{dz} = \left(\frac{A}{wdL}\right)N_{w,x} \quad (8)$$

where the net water flux across the membrane (i.e., the x-direction) is $N_{w,x}$. Water can be transported across the membrane via diffusion, electroosomtic drag, and permeation as expressed below [14]:

$$N_{w,x} = \frac{\rho_M}{M_M\delta_M}\int_{\lambda_+}^{\lambda_-} D_w d\lambda - \left(\frac{\lambda_-}{\lambda_+}\frac{i\xi}{F}\right) - \frac{P_M}{\delta_M}(P_+ - P_-) \quad (9)$$

The membrane water content at the interface of the positive and negative electrodes is related to the activity of water at these locations. For gases in contact with the membrane, the membrane water content is related to the vapor-phase water mole fraction by [14]:

$$\lambda = 123.8y^3_w - 224.01y^2_w + 134.14y_w - 16.35 \quad (10)$$

All other physical parameters in Eq. 9 have been given previously [14].

Similarly, the mole balances for HBr and Br_2 in the positive electrode in the z-direction are given by Eqs. 11 and 12, respectively.

$$\frac{dN_{HBr}}{dz} = -\left(\frac{A}{wdL}\right)\frac{i}{F} \quad (11)$$

$$\frac{dN_{Br_2}}{dz} = \left(\frac{A}{wdL}\right)\frac{i}{2F} \quad (12)$$

Equations 11 and 12 assume that neither of the bromine species crosses the membrane. This assumption was confirmed for the HCl [10] and bromine [9] systems. When HBr and Br_2 dissolve in the aqueous solution (as outlined below), mole balances for these species in the liquid phase need to be added to Eqs. 11 and 12, analogous to what was done previously [10] (details are not given here, but can be seen in the reference). A similar mole balance for H_2 in the negative electrode can be written.

A significant complication occurs in the cell when the composition of water exceeds the dew point, causing condensation. This situation occurs more readily on the Br_2/HBr (i.e., positive) side of the cell as illustrated in Fig. 2. This figure shows the vapor–liquid equilibrium (i.e., dew point) curves generated by the OLI software for the H_2O–HBr (solid lines) and H_2O–H_2 (dotted lines) systems [15]. For example, at 80 °C (353 K) condensation occurs in H_2O–H_2 when the mole fraction of water in the gas phase reaches $y_{w,e} = 0.44$. The resulting liquid is essentially pure water ($x_{w,e} = 1.0$). However, in H_2O–HBr system when the vapor mole fraction of water reaches only $y_{w,e}$ of 0.052, condensation occurs. The resulting liquid is a very strong acid

($x_{w,e} = 0.73$). Bromine has little effect on water condensation in the H_2O–HBr–Br_2 system so the amount of HBr determines the equilibrium compositions for the two phases.

Condensation creates a liquid diffusion barrier that can significantly affect performance. The formation and diffusional resistance of this condensing film was modeled previously [10]. Using this same approach, the concentration of HBr and Br_2 at the catalyst-membrane interface can be calculated by assuming the condensate forms a flowing liquid film within the porous gas-diffusion layer. This film forms at $z = L_c$, which is the point of saturation, and grows linearly as liquid accumulates and eventually flows out of the cell at $z = L$ (see Fig. 1). The expression for the concentration of HBr at the catalyst-membrane interface (C^s_{HBr}) is given in Eq. 13.

$$C^s_{HBr} = C^{eq}_{HBr} - \frac{4C^{eq}_{HBr}}{\pi}\sum_{n=0}^{\infty}\frac{(-1)^n}{(2n+1)} \times \exp\left\{-\frac{D_{HBr}(L-L_c)^2}{V_L\delta_0^2}\left[\frac{(2n+1)\pi}{2}\right]^2\frac{1}{z-L_c}\right\} \quad (13)$$

The OLI software can then be used to calculate the gas-phase mole fraction of HBr and water (y_{HBr}, y_w) that has an equivalent activity to C^s_{HBr} and the corresponding liquid–water activity These quantities are then used in the equilibrium (Eq. 5), membrane (Eq. 10), and kinetic (Eq. 15 below) expressions. An analogous equation to Eq. 13 can be formulated for Br_2.

The overpotential at the hydrogen electrode was measured from the hydrogen pump experiment described previously and fits the follow linear kinetic expression [14]:

$$\eta_- = -0.0062i \quad (14)$$

The relatively small negative-electrode overpotential determined from the hydrogen-pump experiment also incorporates any contact resistances in the cell. Since these losses are small, no attempt is made to differentiate the kinetic losses from other resistances.

The overpotential at the bromine electrode is calculated using the following Butler-Volmer equation.

$$i = i_0\left[\frac{y_{HBr}}{y_{HBr,ref}}\exp\left(\frac{\alpha F}{RT}\eta_+\right) - \frac{y_{Br_2}}{y_{Br_2,ref}}\exp\left(-\frac{\beta F}{RT}\eta_+\right)\right] \quad (15)$$

The reference states are defined as the mole fractions of HBr and Br_2 of 0.5.

The membrane resistance used in Eq. 4 is calculated as described previously [14] and given in Eq. 16 below:

$$R_A = \int_0^{\delta_M}\frac{dx}{\sigma(\lambda)} \quad (16)$$

where the membrane conductivity, σ, is a function of water content and given by [14]:

$$\sigma = 0.0012\lambda^2 - 0.0083\lambda \quad (17)$$

Finally, the applied current density must equal to the integral of the local current density.

$$i_{app} = \frac{\int_0^L i\,dz}{L} \quad (18)$$

This constraint coupled with the equations described above allows one to calculate the cell voltage as a function of the applied current density. The only remaining physical parameters yet to be determined are i_0, α, and β found in Eq. 15. These will be determined by fitting modeling simulations to the current–voltage data collected previously on the Br_2–H_2 redox battery [9]. In this experiment, the membrane electrode assembly (MEA) was used as received from Lyntek, Inc., with an active area of 10 cm^2. This MEA consisted of a Nafion 212 membrane (designated N212) and contained 2.0 mg/cm^2 of Pt black on each side. The positive electrode was fed with different molar ratios of Br_2 to HBr, designated by the parameter r, and the negative electrode was saturated hydrogen. The input HBr molar flow rate was approximately 1.98×10^{-2} mol/(s·cm^2), and the cell was operated at 80 °C and 1 atm. The cell temperature was controlled at 80 °C by heating rods and thermocouples in the cell.

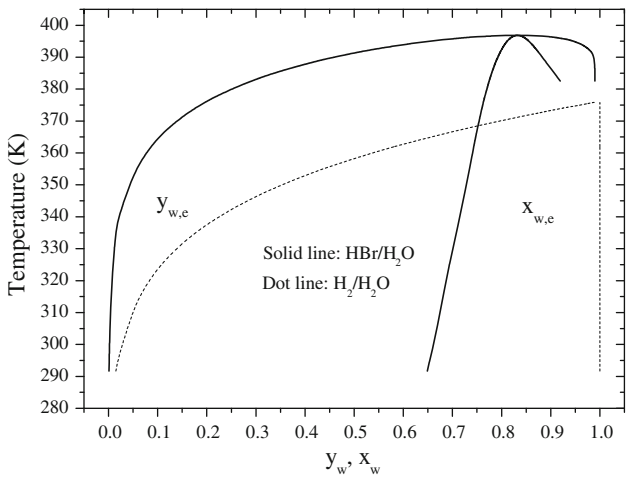

Fig. 2 The vapor–liquid equilibrium (i.e., dew point) curves for the H_2O–HBr and H_2O–H_2 systems generated by the OLI software [15]

3 Results and discussion

Current interrupt experiments, as described previously [14], were used to measure the membrane resistance, R_A, as a function of the applied current density. These data are plotted in Fig. 3 (symbols). Also shown in this figure is

the membrane resistance predicted by the model (solid line). Figure 3 confirms that the parameters measured previously for other systems to predicted membrane resistance (e.g., Eq. 16) are valid here too. Here we see that the membrane resistance increases from 0.085 to 0.145 Ω cm^2 when the current density increases from 0.2 to 2.8 A/cm^2. As the current increases, the average water content of the membrane decreases, thus decreasing its average conductivity.

Figure 4 shows the current–voltage data on charge (open symbols) and discharge (filled symbols) for different values of r (Br_2 to HBr ratio) obtained previously [9]. Also shown in Fig. 4 are the model simulations fit to these data by adjusting the kinetics parameters i_0, α, and β in Eq. 15. The parameter values that resulted in the best fit of simulations to data are listed in Table 1. Both model simulations and experimental data show that higher currents can be reached on charge, and that feed composition can affect performance, especially when reactant composition is low (i.e., low values of r on discharge). Discharge is affected more by condensation since Br_2 (reactant in discharge mode) has a much lower solubility in water than HBr (reactant in charge mode) [15]. Also, condensation occurs more readily on discharge because electro-osmotic drag pulls water towards the positive electrode in this mode.

The model results are further verified in Fig. 5 by comparing simulations to data collected previously in electrolyzer mode [13]. These data were collected under similar conditions to those used to collect the data in Fig. 4 except liquid water was fed to the negative electrode (i.e., no hydrogen), the positive electrode was fed with pure HBr (r = 0), and the HBr flow rate varied with current such that the molar conversion of HBr was maintained at 50%.

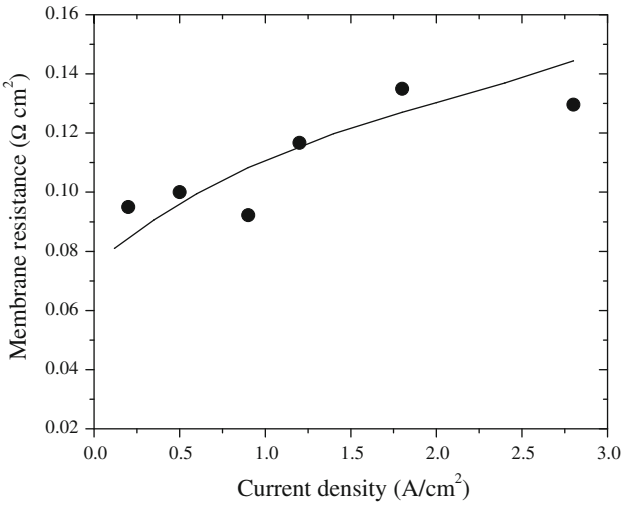

Fig. 3 Comparison of the membrane resistance in N212 from the current interruption and the model prediction. The membrane resistance is measured when the flow battery is run in the charge mode (HBr electrolyzer) at 80 °C with N212

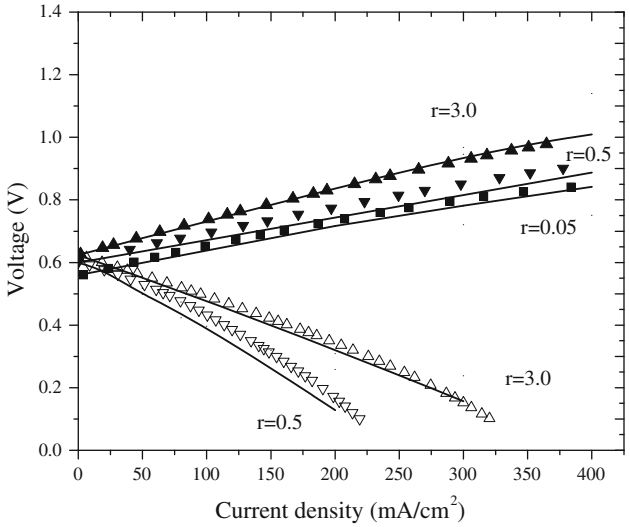

Fig. 4 Simulations (*lines*) and experimental data (*symbols*) [9] of the polarization curves for different values of the inlet gas concentration $r = (y_{Br_2}/y_{HBr})$. The filled symbols represent the charge mode and the open symbols represent the discharge mode. The membrane was Nafion 212 and the cell was maintained at 80 °C and 1 atm

Table 1 Parameters values used in the simulations

Parameter	Value	Ref.
A	10 cm^2	Measured
D_{HBr}	2.08×10^{-5} cm^2/s	[8]
D_{Br_2}	1.31×10^{-5} cm^2/s	[8]
d	0.1016 cm	Measured
i_0	0.08 A/cm^2	Fit to data
L	63.37 cm	Measured
M_M	1,100 g/mol	[9]
w	0.07874 cm	Measured
δ_M	0.005080 cm	Measured
α	0.23	Fit to data
β	0.56	Fit to data
ρ	0.972 g/cm^3	OLI
ρ_M	1.97 g/cm^3	[9]
ξ	2.5	[13]
μ	0.355 cp	OLI

Under these conditions, the applied current density could be run up to 1.7 A/cm^2 without deviating from a linear polarization curve. Again we see that the simulated cell voltage (top solid line) match the data (filled symbols) very well. Also shown in Fig. 5 are the simulated activation overpotentials at the positive and negative electrode, the equilibrium potential, and the Ohmic losses in the cell. It is seen that the activation overpotential at the positive electrode is the largest voltage loss, followed by the Ohmic losses of the membrane. As expect, the negative hydrogen electrode does not contribute much to the cell voltage.

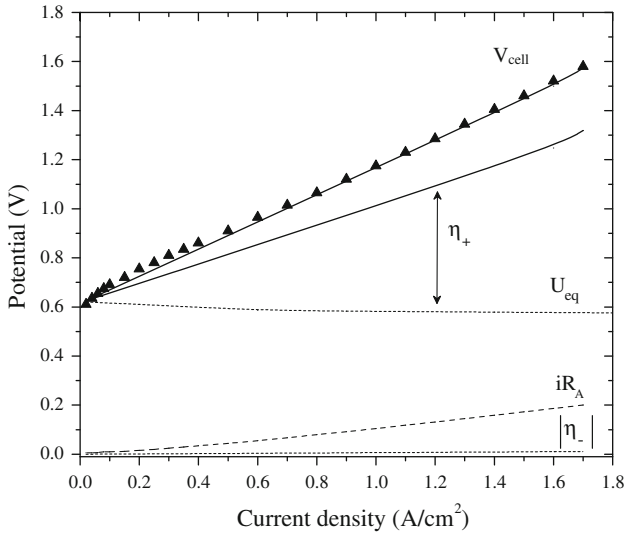

Fig. 5 Individual potentials versus current density simulated from the model. The cell voltage is from data (*filled symbols*) collected previously in electrolyzer mode [13]

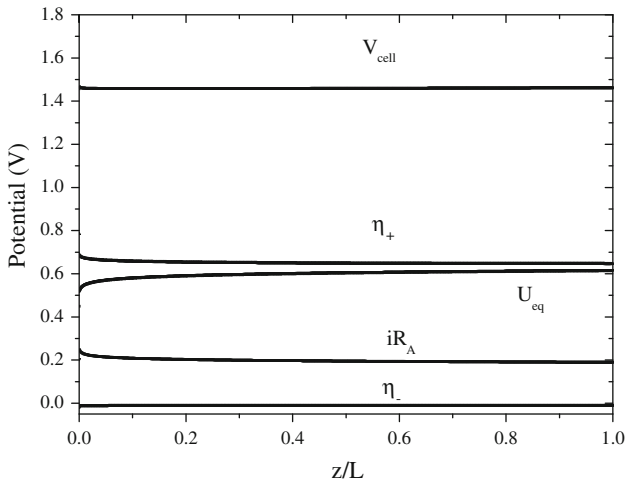

Fig. 6 Distribution of potentials in the direction of flow in the charge mode at 1.6 A/cm^2. All other operating conditions are those used to collect the data shown in Fig. 5

To provide insight into the operation of the cell in Fig. 5, the axial distributions of potentials (Fig. 6), reaction current densities (Fig. 7), vapor-phase water mole fractions (Fig. 8) and the water contents at the membrane/positive-electrode interface (Fig. 9) are provided. Figure 6 shows potential distributions on charge at 1.6 A/cm^2. The cell voltage is assumed constant, and the other values vary down the length of the channel. The equilibrium voltage increases slightly along the channel as the Br_2 concentration increases and the HBr concentration decreases. The higher reactant concentration at the inlet also results in larger currents in this region (see Fig. 7), which in turn

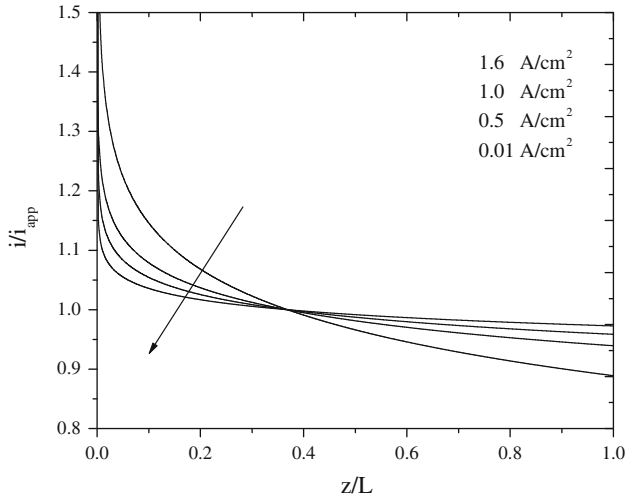

Fig. 7 Distribution of reaction current in the direction of flow in the charge mode. All other operating conditions are those used to collect the data shown in Fig. 5

gives slightly larger positive-electrode overpotentials and Ohmic losses across the membrane at the inlet.

The distributions of reaction current densities at different applied currents are shown in Fig. 7. For all applied currents, the reaction current densities are highest at the entrance to the cell, and decreases exponentially as reactant is consumed. These current distributions are normalized with respect to the applied current so the relative distribution is less uniform at lower currents. The effect of applied current on the normalized current distribution is strongly influenced by the vapor-phase water mole fraction at the positive electrode (Fig. 8). At low currents, the vapor-phase water mole fraction increases rapidly and the condensing line (i.e., dew point) occurs close to the cell inlet. For example, at 0.5 A/cm^2 condensation starts to occur less than 10% into the cell, but at 1.0 A/cm^2 condensation starts 24% into the cell. At applied currents greater than 1.4 A/cm^2, the vapor leaves the cell slightly below the dew point and condensation is completely avoided. Therefore, the reactant concentration, and hence the reaction current, is less uniform at low currents.

The vapor-phase water mole fraction at the positive electrode also influences the membrane resistance by affecting the membrane water content. Figure 9 shows the distribution of the membrane water content at the membrane/positive-electrode interface for different applied currents. Condensation, which occurs at applied currents less than 1.4 A/cm^2, dramatically increases the water content of the membrane. Therefore, the resistance of the membrane is lower at lower currents. At currents greater than 1.4 A/cm^2, condensation is avoided and the water content at the membrane/positive-electrode interface remains relatively constant at approximately 2 over most

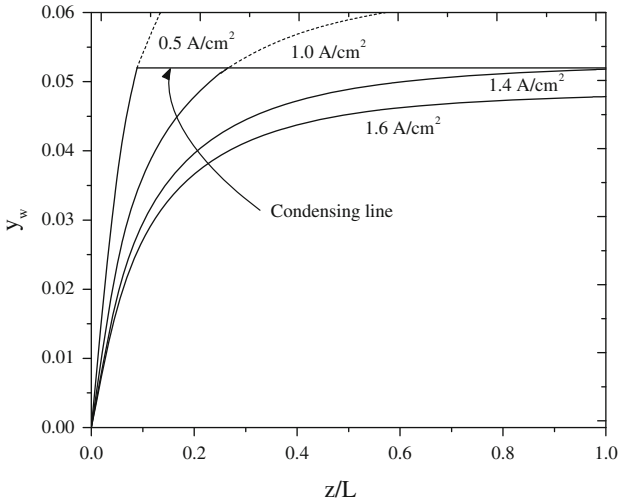

Fig. 8 Distribution of vapor-phase water mole fractions in the direction of flow in the charge mode. All other operating conditions are those used to collect the data shown in Fig. 5. The dash portions of the curves show the water mole fraction if condensation had not occurred

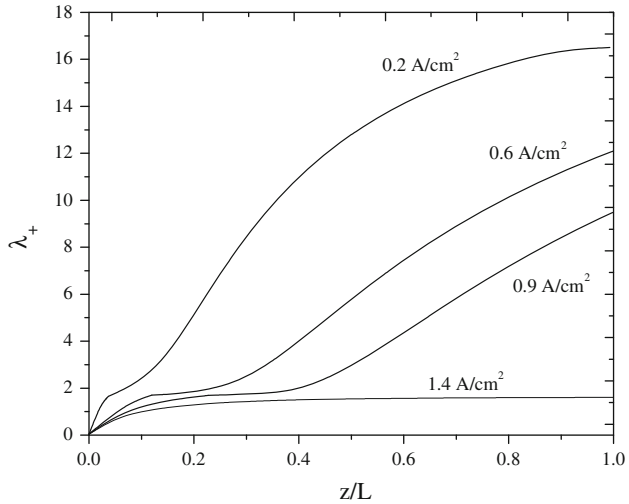

Fig. 9 Distribution of the water content in the membrane at the positive electrode in the direction of flow in the charge mode. All other operating conditions are those used to collect the data shown in Fig. 5

of the channel length. This leads to a lower average membrane water content and a higher resistance. At all currents though, the average membrane water content increases down the length of the channel. Therefore, the membrane resistance decreases down the length of the channel, causing the Ohmic losses to increase slightly towards the cell inlet, consistent with Fig. 6.

Even though the average water content of the membrane decreases (i.e., membrane resistance increases) when condensation is avoided, mass-transfer resistance (and hence charge transfer resistance) is dramatically reduced when condensation is avoided. Therefore, it is important to avoid condensation during cell operation, especially on discharge. As seen in Fig. 8, condensation can be avoided under these operating conditions by applying cell currents greater than 1.4 A/cm^2.

Another operating parameter then can be adjusted to avoid condensation is the pressure differential across the membrane. Figure 10 shows the maximum pressure differential (i.e., $P_+ - P_-$) on charge and discharge needed to avoid condensation as a function of applied current. These pressure differentials are maximums because the curves were simulated with excess HBr (low r values), and hence under conditions when the least amount of water vapor can cause condensation. From Fig. 10, a charging current greater than 1.32 A/cm^2 does not require any pressure differentials (i.e., see Fig. 8). At a current of 0.5 A/cm^2, a pressure differential of 2 MPa can avoid condensation. On discharge, a great pressure differential for a given applied current is needed to ensure condensation is avoided. For example, at 0.5 A/cm^2 a pressure differential of 4.5 MPa

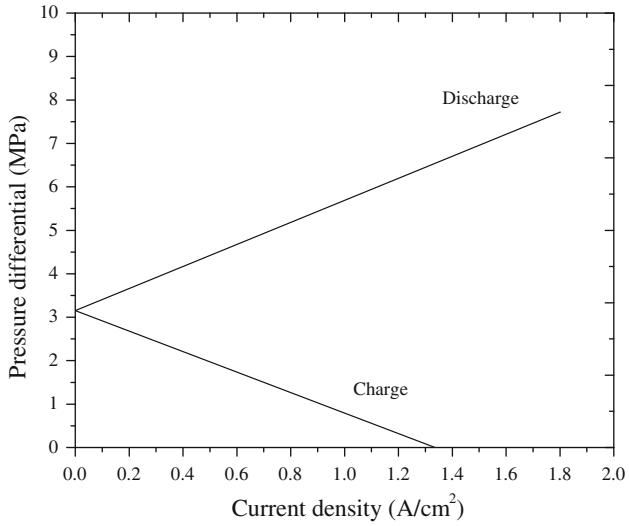

Fig. 10 Maximum pressure differential needed to prevent condensation at the negative electrode. Operating conditions are those used to collect the data shown in Fig. 4

may be needed. Condensation occurs more readily on discharge because electro-osmotic drag pulls water towards the positive electrode in this mode.

Figure 11 shows the resulting current–voltage curves simulated using the pressure differentials shown in Fig. 10. In the absence of condensation, both charge and discharge can exceed 1.4 A/cm^2 at reasonable voltages. This is consistent with experimental data previously collected on charge [12, 13] and shown in Fig. 5. The V–I curves shown in Fig. 11 were generated such that for each current the inlet–outlet conditions on charge were the same as the outlet-inlet conditions on discharge. Specifically, the inlet

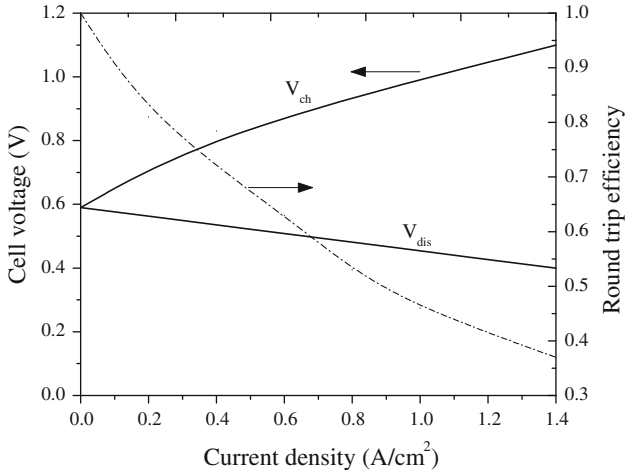

Fig. 11 Current-voltage curves and round trip efficiency (i.e., V_{dis}/V_{ch}) for the H_2/Br_2 flow battery operated without condensation. That is, the pressure differential given in Fig. 10 is used. The r value for charge and discharge is 0.1 and 0.7, respectively, with a flow rate such that the molar conversion of HBr is 50%. All other operating conditions are those used to collect the data shown in Fig. 4

r values for charge and discharge were 0.1 and 0.7, respectively, with a flow rate such that the molar conversion of HBr was 50%. This results in outlet r values for charge and discharge of 0.7 and 0.1, respectively. Therefore, the resulting round-trip efficiencies shown in Fig. 11 are just the ratio of discharge voltage (i.e., energy out) to charge voltage (i.e., energy in), with the system returning its initial state. For example, at 0.5 and 1.4 A/cm^2, the round-trip efficiencies are approximately 63 and 37%, respectively [i.e., $V_{dis}/V_{ch} = (0.52\ V/0.82\ V) = 0.63$; $V_{dis}/V_{ch} = (0.40\ V/1.10\ V) = 0.37$]. Liquid-phase systems can not achieve these currents densities.

Finally, the values shown in Fig. 10 and used in Fig. 11 are meant to illustrate that pressure differential can be used to avoid condensation and significantly improve performance over a range of conditions. The maxiumum pressure differentials needed to avoid condensation at a given current are of course a strong function of the design (e.g., membrane type and thickness) and operating (e.g., temperature, gas flow rate and composition) conditions. This model can be used to estimate the operating conditions needed to take advantage of this gas-phase system.

4 Conclusions

The operation of a gas-phase Br_2–H_2 flow battery is analyzed via a mathematical model and compared to experimental data. The model predicts the operating conditions of the cell in both fuel-cell (i.e., discharge) and electrolysis (i.e., charge) mode as a function of current, inlet gas composition, flow rate, and pressure differential across the membrane. The analysis reveals that gas-phase Br_2/HBr reactants significantly enhance mass transfer, which enables higher currents densities to be achieved compared to a liquid-fed system. A key feature of the model is water transport across the membrane, which determines membrane conductivity, reactant concentration and undesired condensation. The model was then used to provide insight into cell operation, including operating conditions needed to avoid water condensation. For example, operating at pressure differentials where condensation is avoided, the model predicts current densities of 1.4 A/cm^2 on both charge and discharge, and round-trip efficiencies of approximately 63 and 37% at current densities of 0.5 and 1.4 A/cm^2, respectively.

References

1. de Leon CP, Frias-Ferrer A, Gonzalez-Garcia J, Szanto DA, Walsh FC (2006) J Power Sources 160:716
2. Yang Z, Zhang J, Meyer MCWK, Lu X, Choi D, Lemmon JP, Liu J (2011) Chem Rev 111:3577
3. Skyllas-Kazacos M, Chakrabarti MH, Hajimolana SA, Mjalli FS, Saleem M (2011) J Electrochem Soc 158:R55
4. Mitlitsky F, Myers B, Weisberg AH (1998) Energy Fuels 12:56
5. Savinell RF, Fritts SD (1998) J Power Sources 22:423
6. Eustace DJ (1980) J Electrochem Soc 127:528
7. Donepudi VS, Conway BE (1984) J Electrochem Soc 131:1477
8. Madar MJ, White RE (1986) J Electrochem Soc 133:1297
9. Zhang R, Stanford T, Wolters L; Weidner J (2011) Electrochemical and solid-state letters (under review)
10. Motupally S, Becker AJ, Weidner JW (2002) J Electrochem Soc 149:D63
11. Motupally S, Mah DT, Freire FJ, Weidner JW (1998) Interface 7:32
12. Sivasubramanian P, Ramasamy RP, Freire FJ, Holland CE, Weidner JW (2007) Int J Hydr Energy 32:463
13. Zhang R, Weidner JW (2011) Int J Hydr Energy (in press). doi: 10.1007/s001090000086
14. Staser JA, Weidner JW (2010) J Electrochem Soc 157:B952
15. Environmental Simulation Program, OLI Systems Inc., Murray Plains, NJ, USA